Research Square

Preprints are preliminary reports that have not undergone peer review.
They should not be considered conclusive, used to inform clinical practice,
or referenced by the media as validated information.

The indole-3-propionic acid-producing bacteria Clostridium sporogenes protects against influenza

Séverine Heumel
Univ. Lille, CNRS, Inserm, CHU Lille, Institut Pasteur de Lille, U1019-UMR 9017 - CIIL - Centre d'Infection et d'Immunité de Lille

Francis Giraud
Université Clermont Auvergne, CNRS, Clermont Auvergne INP, ICCF

Clément Bordas
Univ. Lille, CNRS, Inserm, CHU Lille, Institut Pasteur de Lille, U1019-UMR 9017 - CIIL - Centre d'Infection et d'Immunité de Lille

Clara valentin
Univ. Lille, CNRS, Inserm, CHU Lille, Institut Pasteur de Lille, U1019-UMR 9017 - CIIL - Centre d'Infection et d'Immunité de Lille

Lucie Deruyter
Univ. Lille, CNRS, Inserm, CHU Lille, Institut Pasteur de Lille, U1019-UMR 9017 - CIIL - Centre d'Infection et d'Immunité de Lille

Audrey Tarricone
Univ. Lille, CNRS, Inserm, CHU Lille, Institut Pasteur de Lille, U1019-UMR 9017 - CIIL - Centre d'Infection et d'Immunité de Lille

Patricia Brito Rodrigues
Univ. Lille, CNRS, Inserm, CHU Lille, Institut Pasteur de Lille, U1019-UMR 9017 - CIIL - Centre d'Infection et d'Immunité de Lille

Fabrice Anizon
Université Clermont Auvergne, CNRS, Clermont Auvergne INP, ICCF

Pascale Moreau
Université Clermont Auvergne, CNRS, Clermont Auvergne INP, ICCF

Sandrine Belouzard
Univ. Lille, CNRS, Inserm, CHU Lille, Institut Pasteur de Lille, U1019-UMR 9017 - CIIL - Centre d'Infection et d'Immunité de Lille

Sandrine Auger
Université Paris-Saclay, INRAE

Isabelle Wolowczuk
Univ. Lille, CNRS, Inserm, CHU Lille, Institut Pasteur de Lille, U1019-UMR 9017 - CIIL - Centre d'Infection et d'Immunité de Lille

Benjamin Hennart

Univ. Lille, ULR 4483 - IMPECS - IMPact de l’Environnement Chimique sur la Santé humaine

Véronique Robert

Université Paris-Saclay, INRAE

Jean Marc Chatel

Université Paris-Saclay, INRAE

François Trottein

Francois.Trottein@pasteur-lille.fr

Univ. Lille, CNRS, Inserm, CHU Lille, Institut Pasteur de Lille, U1019-UMR 9017 - CIIL - Centre d'Infection et d'Immunité de Lille

---

Article

Keywords:

Posted Date: November 11th, 2026

DOI: https://doi.org/10.21203/rs.3.rs-11293546/v1

License: This work is licensed under a Creative Commons Attribution 4.0 International License.
Read Full License

Additional Declarations:
No competing interests reported.

Tables 1 to 3 are available in the Supplementary Files section.

The indole-3-propionic acid-producing bacteria *Clostridium sporogenes* protects against influenza

Séverine Heumel[1], Francis Giraud[2], Clément Bordas[1], Clara valentin[1], Lucie Deruyter[1], Audrey Tarricone[1], Patricia Brito Rodrigues[1], Fabrice Anizon[2], Pascale Moreau[2], Sandrine Belouzard[1], Sandrine Auger[3], Isabelle Wolowczuk[1], Benjamin Hennart[4,5], Véronique Robert[3], Jean Marc Chatel[3], François Trottein[1,✉]

[1]Univ. Lille, CNRS, Inserm, CHU Lille, Institut Pasteur de Lille, U1019-UMR 9017 - CIIL - Centre d′Infection et d′Immunité de Lille, Lille 59000, France

[2]Université Clermont Auvergne, CNRS, Clermont Auvergne INP, ICCF, F-63000 Clermont-Ferrand, France.

[3]Université Paris-Saclay, INRAE, AgroParisTech, UMR1319 Micalis, Jouy-en-Josas 78350, France

[4]Univ. Lille, ULR 4483 - IMPECS - IMPact de l'Environnement Chimique sur la Santé humaine, F-59000 Lille, France

[5]CHU Lille, Service de Toxicologie et Génopathies, F-59000 Lille, France

✉: Correspondence to francois.trottein@pasteur-lille.fr

Abstract

Gut microbiota, especially bacterial metabolites, play a key role in protecting the lungs against respiratory infections such as influenza A virus (IAV). However, IAV infection can disrupt the gut microbiota, potentially increasing disease severity. Notably, reduced levels of the microbial tryptophan metabolite indole-3-propionic acid (IPA) impair viral control and promote pulmonary inflammation, thereby exacerbating IAV infection. In the current study, we investigated the potential protective effects of *Clostridium sporogenes*, a human anaerobic commensal and IPA producer previously shown to mitigate metabolic, inflammatory, and neurological disorders, but whose effects during respiratory infection remain unexplored. Relative to untreated mice, *C. sporogenes* supplementation was associated with less severe disease, lower pulmonary viral loads, and reduced lung inflammation. *C. sporogenes* administration modulated infection-induced gut dysbiosis and restored systemic IPA levels, which were positively correlated with reduced clinical scores and pulmonary viral loads. IPA and its analogues failed to exert direct antiviral effects in cell-based assays, suggesting indirect effects on immunity or other host-pathogen interactions. The pregnane X receptor, a xenosensor known to be activated by IPA, was not involved in the protection mediated by *C. sporogenes*. Lastly, administration of pasteurized *C. sporogenes* improved influenza outcomes, an effect that also correlated with IPA levels. Collectively, these findings suggest that *C. sporogenes* may represent a promising next-generation probiotic candidate for the prevention or mitigation of acute viral respiratory infections.

Sub heading abstract

This study investigates the potential effect of indole-3-propionic acid (IPA)-producing *Clostridium sporogenes* in experimental influenza. The results showed that live and pasteurized *C. sporogenes* protect against infection, an effect associated with restoration of systemic IPA and independent of the pregnane X receptor, a xenosensor known to be activated by IPA.

Abbreviations

Ccl2, chemokine (C-C motif) ligand 2

CWAS, cumulative welfare assessment score

dpi, day post-infection

DMEM, Dulbecco's Modified Eagle Medium

DPBS, Dulbecco's Phosphate-Buffered Saline

IAA, indole acetic acid

IL, interleukin

ILA indole lactic acid

IPA, indole-3-propionic acid

IAV, influenza A virus

LC-MS/MS, liquid chromatography coupled with tandem mass spectrometry

MaAsLin2, multivariate analysis by linear models 2

MOI, multiplicity of infection

Nuclear magnetic resonance (NMR)

DFT, density functional theory

PFA, paraformaldehyde

PXR, pregnane X receptor

TCID50, tissue culture infectious dose

TMPRSS2, transmembrane serine protease 2

Introduction

Every year, influenza A virus (IAV) affects hundreds of millions of people worldwide, and many succumb to pneumonia or complications beyond the lungs[1]. Seasonal flu alone claims between 200,000 and 600,000 lives annually, with millions more suffering long-term consequences[2]. Beyond these recurring challenges, the appearance of a new, reassorted human-pathogenic IAV strain, that happens roughly every 20 to 30 years, can be devastating[1,3]. A growing body of evidence shows that the gut microbiota plays a key role in respiratory infections, including those caused by IAV[4–7]. Mechanistically, components of the gut microbiota, especially metabolites produced by intestinal commensal bacteria, enter the bloodstream and help prime the lungs to fight the virus, largely by boosting interferon-dependent immunity[8–11]. IAV infection can also disrupt the gut bacterial community, as seen in animal studies[7]. Our research, along with others, has shown that such disruptions can contribute to disease severity and promote local and systemic secondary bacterial infections, which are major causes of death[12–16]. In humans, influenza similarly alters the gut microbiota, though the exact impact on disease outcomes is still unclear[17–19]. Recently, using a multi-omic approach, we identified the microbial tryptophan metabolite indole-3-propionic acid (IPA), whose levels drop significantly during infection, as a potential biomarker of influenza resistance and a target for microbiome-based therapeutic interventions[16]. To investigate the role of gut-derived IPA in influenza, and with a view toward probiotic-based interventions, we examined the potential protective effect of *Clostridium sporogenes* in an experimental model of influenza. The latter is a natural commensal in humans and a well-known producer of IPA[20]. Its supplementation in mice mitigates a variety of metabolic and inflammation-related diseases[21–24]. It also improves nerve regeneration and repair[25] and mitigates cognitive impairement in a mouse model of alzheimer's disease[26]. The potential effects of *C. sporogenes* during infection, including viral pneumonia, have not yet been reported. In the present study, we further examined the mechanism of action of IPA, with particular emphasis on its potential role in mediating protection through the pregnane X receptor (PXR), a nuclear receptor known to be activated by IPA[27–29]. Our data collectively demonstrate that supplementation of live and pasteurized *C. sporogenes* protects against severe influenza and that the effects are independent from PXR. Protection correlated with remodeling of the gut microbiota's composition and with elevated systemic IPA levels. The latter as well as IPA analogues have no direct antiviral effects suggesting that the protective effect of IPA *in vivo* may involve indirect modulation of host response. Collectively, restoring IPA levels through preventive *C. sporogenes* supplementation might represent a promising microbiome-based option to control the severity of influenza.

Materials and Methods

Mice and ethics statement

Specific pathogen-free male C57BL/6J mice were purchased from Janvier (Le Genest-St-Isle, France). PXR deficient (*Nr1i2*$^{-/-}$) mice (backcrossed on the C57BL/6J background) were originally engineered

in Pr. Kliewer's laboratory (Department of Pharmacology, UT Southwestern Medical Center, Dallas, TX)[30]. All experiments complied with the current national and institutional regulations and ethical guidelines (Institut Pasteur de Lille, E59 350 009). Protocols were approved by the regional Animal Experimentation Ethics Committee (Comité d'éthique en expérimentation animale/CEEA 75 - Nord-Pas-de-Calais, France) and the French Ministry of Higher Education and Research (authorization numbers: 00357.03, APAFIS#13743-2018022211144403v2, APAFIS#33193-2021092318476492 and APAFIS #49679-2024052417593516 v5. The use of *Nr1i2*$^{-/-}$ mice in experimental influenza was approved by the ministère de l'ensignement supérieur et de la recherche (OGM A2: A2-0406, dossier DUO n°11146). The animals were euthanized by lethal injection of a barbiturate (Euthasol at 140 mg/kg, corresponding to 0.35 mL/kg of a 400 mg/mL solution, administered intraperitoneally), following anesthesia with 2% isoflurane (flow rate of 4 L/min).

Preparation of *Clostridium sporogenes* and treatment

Clostridium sporogenes ATCC15579 was grown at 37°C in Brain-heart infusion medium supplemented with 0.5% yeast extract (Difco, Detroit, USA), 2 mM acetate, 2 mg/mL fructose and 0.5 mg/ml cysteine HCl (Sigma-Aldrich, Saint-Quentin-Fallavier, France), in an anaerobic chamber (90% N2, 5% CO,2 and 5% H2). Bacteria were washed and pellets were resuspended in Dulbecco's Phosphate-Buffered Saline (DPBS) containing 16% glycerol at 4 x 10^8 CFU/mL. Bacteria were aliquoted and frozen at -80°C until use. To evaluate the effect of *C. sporogenes,* mice were administered daily by oral gavage of *C. sporogenes* suspended in sterile anaerobic vehicle at a dose of 8 x10^7 CFUs over a 14-day period. Treatment began 7 days before infection and continued throughout the infection period. The control group received an equivalent volume of vehicle (DPBS containing 16% glycerol). Another group received treatment with pasteurised *C. sporogenes*. Pasteurization (fresh culture) was obtained after 30 min at 70°C. Analysis of bacterial viability and integrity by microscopy indicated that pasteurization killed 99.99% of the bacteria, while 3-5% of the bacteria were sporulated.

Infection and overall clinical score analysis

Mice were anesthetized via intraperitoneal administration of ketamine (1.25 mg) and xylazine (0.25 mg) diluted in 100 µl of PBS, before being intranasally infected with 50 µL of PBS containing (or not, for mock group) 12 plaque forming units (p.f.u.) of the H3N2 IAV strain A/Scotland/20/1974. Body weight and clinical scores (see Table 1 for clinical scoring criteria) were recorded daily. The overall clinical score, ranging from 0 (normal) to 15, was calculated as the sum of individual parameter scores. Data are expressed as cumulative welfare assessment score (CWAS). Mice reaching clinical score of 9 or higher were considered moribund and euthanized. Body weight was measured daily and recorded as percentage of body weight change from baseline (i.e., on infection day). Mice from both groups were sacrificed at 7 dpi.

Viral load, tissue gene expression, and circulating cytokine levels

To quantify virus load, the left lobe lungs and the right superior and post-caval lobes were homogenized in 1 mL. Virus load in lung homogenates was assessed by titration of 50% tissue culture infectious dose (TCID50) using Madin-Darby canine kidney (MDCK, ATCC CCL-34) cells. Data are expressed as number of viruses per mL. The lung (the right middle and inferior lobes) and the colon were stored in RNAlater® (Ambion, Thermo Fisher Scientific, Waltham, MA) and frozen at -80°C until quantitative RT-PCR analysis. Quantitative RT-PCR was performed on the QuantStudio™ 5 Flex Real-Time PCR System (Thermo Fisher Scientific, Waltham, MA) as described[16]. The murine primer sequences are listed in Table 3. Gene expression levels were normalized to *Gapdh* expression. Serum samples were collected, stored at -80°C and analyzed for cytokine profiles by ELISA (Thermo Fisher Scientific).

Quantification of tryptophan metabolites

Tryptophan metabolites were quantified by targeted LC-MS /MS. Briefly, 50 µL of serum were combined with an equal volume of pure acetonitrile to precipitate proteins. The acetonitrile contained deuterated internal standards at a concentration of 50 µM (CDN Isotopes, Pointe-Claire, QC, Canada). Following centrifugation, 50 µL of the resulting supernatant were diluted with 600 µL of deionized water. A 10 µL aliquot of the diluted sample was subsequently injected into a UPLC-MS/MS system (Acquity TQ-XS Detector, Waters, Milford, MA) fitted with a C18-XB column (1.7 µm, 100 Å, 150 × 2.1 mm; Phenomenex®, Torrance, CA). Analytes were detected in positive ionization mode using multiple reaction monitoring. Data acquisition and processing were performed using MassLynx software (Waters).

***In vitro* anti-viral effects of IPA and IPA analogues**

A549 cells (ATCC, CRM-CCL-185) expressing transmembrane serine protease 2 (TMPRSS2) and MLE12 cells (ATCC, CRL-2110) were cultured at 37°C in Dulbecco's Modified Eagle Medium (DMEM) plus GlutaMAX™ or DMEM/F-12 medium (Gibco, Thermo Fisher) supplemented with 10% fetal calf serum serun (Avantor, Radnor, PA, South America origin). Amantadine, IPA and IPA analogues were dissolved in DMSO at 500 and 800 mM. Each plate contains the negative (DMSO at 0.25%, w/vol) and positive (amantadine at a final concentration of 100 mM, Sigma) controls. Compounds and DMSO were spotted with an Echo acoustic dispenser (Beckman Coulter, USA). One day prior to infection, 10,000 A549-TMPRSS2 cells or 5,000 MLE-12 cells were seeded per well in 384-well plates (Greiner) and incubated overnight at 37°C. On the next day, cells were pre-treated for 1 h with IPA (1-1000 µM) or IPA analogues (75 µM) diluted in DMSO. One hour later, cells were infected with H3N2 IAV strain A/Scotland/20/1974 at 1 multiplicity of infection (MOI). Plates were incubated for 24h at 37°C and then fixed in paraformaldehyde (PFA). After washing, cells were

permeabilized with PBS containing 0.1% (v/v) Triton X-100 for 4 minutes and non-specific sites were blocked with 5% goat serum (Vector Laboratories, Burlingame, CA) for 30 minutes at room temperature. Staining with primary mouse anti-Influenza A Nucleoprotein, clone AA5H (monoclonal) antibody (Tebubio, Le Perray-en-Yvelines, France) was performed at a dilution of 1:1000 in PBS supplemented with 5% goat serum for 30 minutes at room temperature. After three washing with PBS, cells were incubated with secondary antibody, anti-donkey Alexa-Fluor™ 488-conjugated anti-mouse IgG (H+L) at a dilution of 1: 500 in PBS-5% GS supplemented with DAPI/Hoechst (Thermofisher, 1:500) for 30 minutes at RT protected from light. After three washing, the IAV infected cells were measured using an automated high-content fluorescent microscope (IN CELL Analyzer 6000, Molecular Devices) equipped with a 20X (NA 0.75) or 60X (NA 0.95) air objective (Nikon, Tokyo, Japan). Images were then analyzed by using Columbus image analysis software (version 2.3.1, PerkinElmer) to determine the number of infected cells (N-positive cells) and the total number of cells (DAPI stained nuclei).

Synthesis of conformationally constrained IPA analogues

A short previously reported synthetic strategy was applied to build a new library of IPA analogues (Figure 3C). Starting from simple commercially available indoles with bromine atoms at various positions of the carbocycle, reaction with itaconic anhydride in the presence of $BF_3{\cdot}Et_2O$ afforded carboxylic acid analogues **1**–**4** in moderate to good yields. To check the impact of the introduction of a halide atom on the activity, the same method was used with 4-fluoroindole as starting material leading to compound **5**. Direct isolation of pure carboxylic acids **2** and **3** as easy-to-handled powders from step one was tedious. To bypass this trouble in these two particular cases, an indirect synthetic route was applied. Crude reaction mixtures from the first step were engaged with refluxing methanol or ethanol generating the corresponding esters **8** and **11** which were further hydrolyzed without purification using concentrated HCl aqueous solution, to afford the desired acids **2** and **3** as solids after simple filtration. To enlarge our structure-activity relationship study, modulations were also introduced on the carboxylic acid part. Thus, in a second step, Fischer esterification in refluxing methanol or ethanol afforded corresponding esters **6**–**15** in good yields. Finally, in order to evaluate the influence of the hydrogen atom at the N1-position on the biological activity, compounds **16**–**25** were synthesized using iodomethane in the presence of sodium hydride, with yields ranging from 24% to 73% (Figure 3C).

Structure and mechanism elucidation

The first cyclization step leading to compound **1**–**5** proceeds by initial conjugated addition of indole to the double bond of itaconic anhydride giving intermediate **26** (Supplementary Figure 4)[31]. Further 1,2 attack at one carbonyl to generate a spiro-indole, and 1,2-migration produces the tetrahydrocarbazole scaffold. 4-oxygenated isomer is also a possible product of the reaction. Although ^{1}H and ^{13}C NMR spectra of compounds **1**–**25** were consistent with the proposed structure having the ketone function at

the 1-position, we sought to further validate these structural assignments by performing DFT calculations of the ^{13}C NMR chemical shifts for compound **7** and its 4-oxo isomer **7'** (Supplementary Figure 4). The calculated chemical shifts were then compared to the experimental ones obtained for **7** whose ^{13}C NMR signal assignments were established on the basis of ^{1}H, ^{13}C, HSQC ^{1}H–^{13}C, HMBC ^{1}H–^{13}C, COSY ^{1}H–^{1}H and NOESY ^{1}H-^{1}H experiments. The computed ^{13}C NMR chemical shifts (Table S1) for compound **7** showed excellent agreement with the experimental data, with RMSD values of 2.3 ppm (C5, bonded to bromine was excluded from the RMSD calculation). In contrast, comparison of the experimental data with the chemical shifts calculated for **7′** gave significantly higher RMSD values of 7.2 ppm. The discrepancies were particularly pronounced for C4a and C9a, for which differences of 15-20 ppm were observed for **7′**, compared with approximately 2 ppm for **7**. Taken together, the low RMSD obtained for compound **7** and the clear discrimination from the alternative isomer confirm the structure of the compound (Supplementary materials and methods).

Analysis of PXR expression by immunohistochemistry

Paraffin-embedded lung sections were deparaffinized using the PT Module and Dewax and heat-induced antigen retrievial Buffer H, pH 9.0 (Epredia, Portsmouth, NH). Immunohistochemical labelling was performed on the Autostainer 360-2D (Epredia). The slides were immersed in PBS-Tween 20 buffer (PBT010, SkyTek Laboratories) for 15 min, washed, and then blocked with EZ Block solution (EZB125, SkyTek Laboratories, Logan, Utah). For immunolabeling, sections were incubated overnight at 4°C with the polyclonal rabbit anti mouse-PXR (ab217375, Abcam) diluted 1:100 in normal antibody diluent (EZB 125, SkyTek Laboratories). The sections were then washed with PBS-Tween 20 buffer and then incubated for 1 h with the biotinylated, goat anti-rabbit IgG HRP-labelled polymer (BA-1000, Vector Laboratories, Newark, CA). After washes, slides were incubated with the avidin-biotin-HRP (ABC) complex (Vector Laboratories) for 45 min. After washes, tissue sections were stained with diaminobenzidine (ImmPACT DAB EqV, Peroxidase substrate, SK-4103, Vector Laboratories), counterstained with hematoxylin, dehydrated through graded alcohols, and mounted with coverslips. The entire tissue sections were scanned using Axioscan Z1 (Zeiss, Germany) and then subjected to digital image analysis using QuPath open software for bioimage analysis (https:// qupath. github. io). Cells were classified as either positive or negative based on the average intensity of nuclear DAB staining.

Sample collection, genomic DNA extraction and sequencing

Genomic DNA extraction from feces was conducted by classical procedure using the QIAamp®PowerFecal®Pro DNA Kit from Qiagen (Les Ulis France). Genomic DNA suspensions were stored at -20°C. Microbial diversity and composition were determined for each sample by targeting a portion of the ribosomal genes. Amplification of the V3 and V4 hypervariable region of the 16S rRNA gene was performed using the Kit PCR KAPA HIFI HotStart from Kapabiosystem (Le Cap,

South Africa). The PCR products were multiplexed at equal concentrations and purified using a PippinHT system (Sage Science, Beverly, MA). Sequencing was performed using a 250-bp paired-end sequencing protocol on the @BRIDGe plateform (INRAE, Jouy en Josas, France) using MiSeq M04152 Illumina (Illumina, San Diego, CA).

MaAsLin2 analysis

Differential abundance analyses were performed at the genus level using MaAsLin2[32]. Outliers were identified using Tukey's rule in Aitchison space and excluded before analysis. Genera were retained if they reached a maximum relative abundance ≥1% and a prevalence ≥30% in at least one group. Data were TSS-normalized, log-transformed and analyzed using linear models. Longitudinal models included time as a fixed effect and mouse identity as a random effect, whereas between-group models included treatment as a fixed effect, with vehicle as the reference. Associations with FDR-adjusted $q < 0.25$ were considered significant.

Statistical analysis

Results are presented as the mean ± SD (standard deviation), as indicated. Statistical analyses were performed using GraphPad Prism (version v9.2.0, GraphPad Software Inc., San Diego, CA). A two-tailed Mann-Whitney *U*-test was used to compare two groups. For each mouse, the area under the curve (AUC) for body weight change and clinical score was calculated individually from longitudinal measurements using the trapezoidal method in GraphPad Prism. AUC values were compared between groups using the two-tailed unpaired Mann-Whitney test. Pearson correlation analysis and linear regression were performed using GraphPad Prism (version v9.2.0) to assess the relationship between the concentration of IPA and the number of viruses in lungs. The Pearson correlation coefficient (r), coefficient of determination (R^2), and corresponding two-tailed P value were calculated. Statistical significance was defined as $*p < 0.05$, $**p < 0.01$, and $***p < 0.001$.

Results

Supplementation with *C. Sporogenes* restores the systemic level of IPA and reshapes the composition of the gut microbiota following IAV infection

Adult male C57BL/6 mice (3 months old) were supplemented daily by intragastric administration of *C. sporogenes* or vehicle for seven consecutive days before the inoculation of a sub-lethal dose of IAV. Treatment was administered throughout the duration of the infection (schematic procedure in Figure 1A). Mice were sacrificed at day 7 post-infection (7 dpi), corresponding to the peak of the acute phase. We first investigated whether *C. sporogenes* supplementation impacts on IPA levels in IAV-infected mice. Targeted liquid chromatography coupled with tandem mass spectrometry (LC-MS/MS) revealed IPA in blood at steady state (Figure 1B). As observed previously[16], blood levels of IPA fell massively upon IAV infection. Interestingly, *C. Sporogenes* treatment restored blood IPA concentration at 7 dpi,

although it did not return to basal levels. The concentrations of other tryptophan-derived metabolites such as indole lactic acid (ILA) and indole acetic acid (IAA) were significantly altered by infection (Supplementary Figure 1A and 1B). While IAA levels were unaffected by *C. sporogenes* supplementation, ILA concentrations were significantly reduced following supplementation.

We then investigated whether restoration of IPA levels associates with changes in the composition of the gut microbiota. To this end, 16S rRNA gene amplicon sequencing was performed on fecal samples collected one day before infection and at sacrifice (Figure 1A). We used MaAsLin2 (multivariate analysis by linear models 2) to identify and hierarchically rank the bacterial taxa that contributed most to the discrimination between the groups (genus level). Influenza virus infection altered the composition of the gut microbiota in both vehicle-treated and *C. Sporogenes*-treated mice (Supplementary Figure 1C). Although the overall infection-induced changes were similar between the two groups, supplementation with *C. Sporogenes* was associated with specific alterations, including an increased relative abundance of *Clostridiaceae clostridium*, *Lachnospiraceae anaerotipes*, *Enterococcaceae enterococcus*, and *Desulfovibrionaceae bilophila* (Supplementary Figure 1C, *left* panel). Comparison of vehicle-treated and *C. sporogenes*-treated mice at 7 dpi confirmed the enhancement of *C. clostridium* spp. (Figure 1C). In parallel, the relative abundance of two genera within the *Lactobacillaceae* family, namely *L. lactobacillus* and *L. limosilactobacillus*, was also enhanced (Figure 1C). Together, these findings indicate that *C. sporogenes* supplementation reshapes the composition of the gut microbiota and counteracts the infection-associated decrease in circulating IPA levels. Given the reported important role of IPA during influenza[16], we next investigated whether *C. Sporogenes* supplementation could improve infection outcomes.

Supplementation with *C. Sporogenes* protects against influenza

On average, IAV-infected mice had lost ~ 15% of their initial body weight on 7 dpi (Figure 2A, *left* panel). Supplementation with *C. sporogenes* significantly attenuated the body weight loss resulting from infection (Figure 2A, *right* panel). Clinical score measurement (Table 1 for the analyzed criteria) indicated that *C. sporogenes*-treated mice experienced less severe disease (almost no symptoms) relative to vehicle-treated counterparts (Figure 2B). Interestingly, the reduced body weight loss and clinical scores were positively corelated with systemic IPA levels (Supplementary Figure 2A). Quantification of infectious virus production in lungs indicated that *C. Sporogenes* treatment was associated with a significantly lower viral load at 7 dpi (Figure 2C). This reduced viral load was positively correlated with circulating IPA levels (Figure 2D). It is noteworthy that the kynurenin-to-tryptophan ratio, a predictive marker of influenza severity and mortality[33,34], was significantly reduced in *C. sporogenes*-treated mice (Supplementary Figure 2B). The level of interferon (IFN)-stimulated genes (ISGs), the expression of which is proportional to the virus load at this time, was lower in *C. sporogenes*-treated animals than in vehicle-treated controls (Figure 2E, *left* panel). This included for instance genes encoding the inducible protein Mx1and IFN-γ. The pathogenesis of viral infection is

associated with an excessive inflammatory response. The expression of genes encoding inflammatory genes such as interleukin (IL)-6 and chemokine (C-C motif) ligand 2 (Ccl2) was also reduced in the lungs from *C. sporogenes* treated-mice (Figure 2E, *right* panel). In line, IL-6 concentration in blood was reduced while that of IFN-γ tended to be diminished by *C. sporogenes* administration (Figure 2F). Influenza results in an impairment of the epithelial barrier function[35]. Interestingly, *C. sporogenes* supplementation attenuated the infection-associated reduction in transcripts encoding forkhead box protein J1 (Foxj1, involved in ciliogenesis), claudin-1 and claudin-7 (Cdln1 and Cdln7, components of epithelial tight junctions), and surfactant protein C (Sptpc, a marker of alveolar type 2 epithelial cells) (Figure 2G). These findings suggest that *C. sporogenes* supplementation may contribute to the preservation of the pulmonary epithelial barrier. Influenza infection alters gut homeostasis and promotes intestinal inflammation[24,36]. Interestingly, *C. sporogenes* supplementation lowered the synthesis of transcripts encoding ISGs and inflammatory markers in the colon such as Mx1, Isg15, IFNγ, and IL12p40 (Supplementary Figure 2C). Taken as a whole, *C. sporogenes* supplementation reduced pulmonary viral burden and attenuated lung, systemic, and intestinal inflammation.

IPA and IPA analogues have no direct antiviral activity against IAV *in vitro*

The effect of *C. sporogenes* supplementation on viral load correlates with IPA levels (Figure 2D). The extent to which the observed *in vivo* activity of *C. sporogenes* (this study) and IPA[16] is attributable to their direct antiviral effects *versus* their host immune-modulatory functions remains to be determined. Given that several indole derivatives have been reported to exert direct antiviral effects[37–41], we measured the antiviral activity of IPA and IPA analogues *in vitro*. Given that the serum concentrations of IPA are relatively high under homeostatic conditions (in the micromolar range, 3 μM in our setting), IPA was used at 1, 10, 100 and 1000 μM. Human A549 lung epithelial cells, which represent a primary target of IAV infection, were pre-treated with IPA for 1 h prior to viral infection. Amandatine, used as a positive control, significantly lowered the number of infected cells 24 h post-infection (Figure 3A). In marked contrast, IPA had no effect on viral replication at any of the concentrations tested. Similar data were obtained using the mouse lung epithelial cell line MLE-12 (Figure 3B).

The therapeutic applications of IPA are attracting increasing attention, with ongoing opportunities to optimize its structure for future clinical use[23,42]. We therefore synthesized various analogues of IPA by modifying the indole structure at positions 1, 4, 5, 6, and 7 (Figure 3C). We also added an additional ring to make the molecule more constrained[43]. IPA chemical structure could be optimized on the basis of a large structure-activity relationship study. First of all, as the introduction of various substituents such as halogen atoms on benzenic ring could highly modify the activity of indole derivatives, fluorine and bromine atoms were introduced in 4-, 5-, 6- or 7-positions (**1**-**5**). Then, to evaluate the impact of polar functions on the activity, hydrogens atoms of the carboxylic acid group and the one of the indolic NH moiety were removed leading after Fischer esterification to the corresponding methyl and ethyl

esters analogues (**6**-**15**) or after methylation in basic conditions to N-methylated derivatives (**16**-**25**), respectively. Nuclear magnetic resonance (NMR) calculations confirmed the structure of the compounds in accordance with the original work. Comparison of density functional theory (DFT) 13C calculated chemical shifts and experimental 2D NMR analysis of compound **7** and its regioisomer **7'** evidenced a clear discrimination between both isomers and confirm the structure of the compounds (Table 2 and Supplementary Figure 4). As shown in Figure 3D, these IPA analogues failed to reduce viral replication in our experimental settings. These findings indicate that IPA does not exert a direct antiviral effect against IAV in lung epithelial cells *in vitro*, suggesting that the protective effects observed *in vivo* are more likely mediated through host-dependent mechanisms.

The protective effects of *C. sporogenes* are not mediated by PXR

IPA can signal through the xenobiotic nuclear receptor PXR, encoded by *Nr1i2*[29,44]. The latter plays a key role in regulating the expression of enzymes and transporters involved in drug metabolism following exposure to xenobiotics. PXR is predominantly expressed in the liver and gastrointestinal tract, where it mediates detoxification and anti-inflammatory effects[27–29]. Immunohistochemical analysis revealed PXR expression in the lungs, including in bronchial and alveolar epithelial cells (Figure 4A). Quantitative RT-PCR confirmed *Nr1i2* expression in the lungs and revealed a strongly reduced expression at 7 dpi compared with baseline levels (Figure 4B, *left* panel). Consistently, expression of the PXR target gene *Cyp3a11* was also strongly downregulated at 7 dpi (Figure 4B, *right* panel). *C. sporogenes* supplementation did not prevent the infection-associated decrease in *Nr1i2* and *Cyp3a11* expression at 7 dpi (not shown).

We then assessed the potential contribution of PXR in host response during experimental influenza infection. PXR deficiency (*Nr1i2*$^{-/-}$ mice) had no effect on influenza severity in terms of body weight loss and clinical score, viral load, and expression of ISGs and inflammatory factors (Figure 4C). These findings are consistent with the marked drop of both systemic IPA levels and pulmonary *Nr1i2* expression observed in IAV-infected mice. We next investigated whether the protective effects of *C. sporogenes* were dependent, at least in part, on PXR expression. As shown in Figure 4D, PXR deficiency had no effect on body weight loss, clinical score and viral load. While ISG transcript expression was not modulated by PXR deficiency, expression of inflammatory transcripts tended to be enhanced. We conclude that PXR does not naturally contribute to influenza severity or to the protection conferred by *C. sporogenes* supplementation.

Pasteurized *C. sporogenes* is protective against influenza

Using non-viable bacteria may improve safety while simplifying large-scale production, formulation, and quality control. Indeed, the use of non-viable bacteria could offer important safety advantages over administration of live bacteria, while also facilitating manufacturing, formulation, and quality control at an industrial scale. Given the therapeutic potential of *C. sporogenes* for human

applications[21–23,25,26,45], we therefore evaluated whether pasteurized *C. sporogenes* could similarly mitigate influenza severity. To this end, we adapted a method originally developed for the preparation of pasteurized *Faecalibacterium duncanie*[46]. In the case of *C. sporogenes*, this procedure strongly, but not completely, reduced *C. sporogenes* viability (see Materials and Methods). Mice were treated with pasteurized *C. sporogenes* using the same protocol that was used for the native form (Figure 1A). Similar to the beneficial effect observed with live *C. sporogenes*, and compared to control mice, treatment with pasteurized *C. sporogenes* was associated with a significant attenuation of body weight loss in IAV-infected mice (Figure 5A). In parallel, pasteurized *C. sporogenes* ameliorated clinical scores of IAV-infected mice (Figure 5B). This beneficial effect was associated with a significantly lower viral load in the lungs (Figure 5C). Reduction of viral load, as well as body weight loss and clinical scores, associated with restoration of IPA levels in blood (but not IAA and ILA) (Figure 5D, Supplementary Figure 3A and 3B and not shown). As observed with live *C. Sporogenes*, pasteurized *C. Sporogenes* significantly reduced the concentration of ILA (but not IAA) as well as the kynurenin/tryptophan ratio (Supplementary Figure 3B and 3C). The expression level of gene encoding Mx1, Isg15 and IFN-γ as well as inflammatory markers was lower in mice supplemented with pasteurized *C. sporogenes* than in control mice (Figure 5E). The blood concentrations of IFN-γ and IL-6 were low in *C. sporogenes*-treated mice (Figure 5F). Unlike live *C. sporogenes*, pasteurized *C. sporogenes* failed to modulate the expression of genes involved in lung barrier (Figure 5G). On the other hand, expression of transcripts encoding ISGs and inflammatory cytokines was abrogated in the colon (Supplementary Figure 3D). Comparison of the gut microbiota's composition between vehicle-treated and pasteurized *C. sporogenes*-treated mice at 7 dpi revealed higher abundance of *C. clostridium* and members of the *Lactobacillaceae* family in the latter group (Figure 5H). Taken together, pasteurized *C. Sporogenes* is almost as effective as live *C. Sporogenes* in lowering influenza severity.

Discussion

Recent findings from our group indicate that IPA is a key factor in modulating the severity of experimental influenza[16]. Notably, a recent study confirmed this finding[47], and additional studies suggest that the beneficial effects of IPA may extend to other viral pneumonias in humans, including coronavirus disease 2019[47–49]. These findings collectively raise the possibility that the capacity of the gut microbiome to produce IPA from tryptophan may serve as a biomarker of susceptibility to severe viral pneumonia. In support of this hypothesis, a recent large-scale human study involving more than 13,000 participants demonstrated that higher IPA levels are associated with a lower risk of developing (bacterial) pneumonia[50]. Consequently, supplementation with IPA-producing bacteria, or with bacteria that enhance IPA synthesis, could represent a promising strategy to reduce the severity and perhaps long-term consequences of pneumonia. In the current study, we demonstrate that *C. sporogenes*, a spore-forming bacteria known to produce IPA, protects against acute influenza in mice, revealing its

potential as a prophylactic and therapeutic strategy to mitigate post-viral pneumonia complications through the gut-lung axis.

Clostridium sporogenes has strong potential for clinical application[21–23,25,26,45]. However, to our knowledge, its impact on infectious diseases, including respiratory viral infections, has not yet been investigated. Likewise, although the beneficial effects of probiotics, primarily *Lactobacillus* and *Bifidobacterium* spp., on influenza have been widely reported[51–53], the potential role of tryptophan derivatives remains elusive. Our data clearly demonstrated that preventive use of live and pasteurized *C. sporogenes* protects against influenza. The substantial reduction in viral replication (>2-log decrease at 7 dpi) likely accounts for the strong reduction in both local and systemic inflammation. However, the possibility that *C. sporogenes* also exerts direct anti-inflammatory effects, independently of its antiviral activity, cannot be ruled out. Consistent with this hypothesis, *C. sporogenes* has been reported to attenuate inflammation in multiple inflammatory conditions[21,22,26]. Remarkably, protection confered by *C. sporogenes* strongly associated with IPA levels. It is noteworthy that IAA and ILA, other microbial tryptophan metabolites, did not correlate with disease outcome in our setting. Considering that *C. sporogenes* possesses a specific metabolic fingerprint, consisting predominantly of IPA, the branched-chain acids isobutyrate and isovalerate and the short-chain fatty acids propionate and acetate (the latter has also been shown to protect against influenza severity[14,54]), it remains possible that metabolites other than IPA, or additional bacterial factors, contribute to the observed protection. *C. sporogenes* treatment increased the relative abundance of two important genera within the *Lactobacillaceae* family, namely *L. lactobacillus* and *L. limosilactobacillus*, which are well known for their beneficial effects on health. It is noteworthy that some members of the *Lactobacillaceae* family can produce ILA, which can serve as a precursor for microbial IPA production[55]. Consistent with a potential microbial cross-feeding mechanism, ILA levels were reduced in *C. sporogenes*-treated mice.

Clostridium sporogenes and IPA exert their effects through diverse mechanisms involving both receptor-dependent pathways, such as those triggered by PXR, the aryl hydrocarbon receptor, and peroxisome proliferator-activated receptor-β/δ, and receptor-independent mechanisms[21,24,29,42,45,56]. Of note, PXR has recently been shown to protect against acute respiratory distress syndrome via indole-3-acetaldehyde[57]. Our findings indicate that *C. sporogenes* (and IPA, not shown) protects against influenza independently of PXR, suggesting that alternative pathways mediate their beneficial effects. These mechanisms remain to be fully elucidated. In the same line, and in our experimental setting, the mode of action of IPA on the control of viral load remains to be elucidated. The effect could be direct, targeting viral proteins or host cellular pathways involved in viral entry, replication, assembly, or release, or indirect, through modulation of innate or adaptive immunity, inflammation, epithelial responses, or other host-pathogen interactions. It is noteworthy that IPA can activate innate responses,

for instance by activating signal transducer and activator of transcription-related pathways and inducing interferon type 1 production (*e.g.*, by epithelial cells)[23,47]. Our data show no direct effect of IPA on IAV replication *in vitro*, contrasting with the findings of Antunes and colleagues[47]. This discrepancy may reflect differences in experimental models, as their study used primary cells and tissues, whereas ours relied on cell lines. Although cell lines are valuable for investigating viral replication and antiviral mechanisms, they do not fully recapitulate the complexity of host tissues, often exhibit altered metabolism and antiviral responses, and lack interactions with immune cells and inflammatory mediators that can influence antiviral activity.

The development of IPA as a target drug for the treatment of intestinal, metabolic and neuronal diseases is promising[23,42]. Although IPA research is still in the experimental animal model stage, there is growing interest in the many therapeutic applications of IPA and increasing opportunities to further modify IPA for future clinical applications. In this study, given the potential antiviral effects of indole derivatives[37–41], we performed a structure-activity relationship study around the IPA scaffold. Diverse substituents were introduced on the indole benzo ring and nitrogen atom, as well as on the carbonyl function. NMR calculations confirmed the structure of the compounds. In our setting, IPA analogues failed to exert a direct effect on viral replication *in vitro*. Whether IPA analogues can reduce viral load *in vivo* remains to be investigated. An important finding of the current study is that pasteurized *C. sporogenes* is efficient in protecting against influenza infection. 16S rRNA sesquencing analysis indicated that pasteurisation does not prevent the growth of *C. sporogenes* (analyzed 14 days after treatment initiation) and protection correlated with blood IPA levels. It is likely that surviving spores returned to vegetative growth after pasteurization. It is noteworthy that unlike live *C. sporogenes*, pasteurised *C. sporogenes* had no apparent effect on pulmonary barrier functions. The reasons remain unclear and warrant further investigation. The fact that pasteurized *C. sporogenes* exhibited effects similar to those of live bacteria in mitigating influenza severity, with the exception of effects on the pulmonary barrier, is particularly exciting from a therapeutic perspective. Indeed, the use of non-viable bacteria could offer important safety advantages over administration of live bacteria, while also facilitating manufacturing, formulation, and quality control at an industrial scale.

Collectively, restoring IPA levels through preventive *C. sporogenes* supplementation might be an interesting strategy for limiting the severity of influenza. These findings may also extend to other respiratory viral infections, such as severe acute respiratory syndrome coronavirus 2 and respiratory syncytial virus[47–49]. Additionally, given the growing interest in the role of IPA in bacterial infections, including bacteria-associated pneumonia[29,50,58,59], preventive *C. sporogenes* supplementation to restore IPA levels may represent a promising approach in these settings as well. The present study has some limitations. First, we focused on male mice and the potential benefit of *C. sporogenes* treatment in female mice, known to show more acute outcomes[60], needs to be investigated. Another limitation is

our focus on the acute phase of infection. Given that severe influenza can lead to long-term sequelae as a result of excessive inflammation and/or defective recovery/repair processes, the potential impact of *C. sporogenes* treatment on these sequelae warrants further investigation. Our study was limited to the assessment of lung, and to a lesser extent, gut damage. Future research should explore the broader impact of *C. sporogenes* supplementation, examining its potential to alleviate both pulmonary dysfunction and extrapulmonary conditions, including skeletal muscle atrophy that restricts mobility, cardiac and renal damage, and cognitive deficits. Lastly, we specifically investigated the effects of a preventive strategy designed to deliver *C. sporogenes* before infection, thereby potentially influencing gut microbiota functionality and/or programming host cells to fight against infection. *C. sporogenes* was also delivered during the early phases of infection. Whether therapeutic delivering *C. sporogenes* at symptom onset could provide benefits and further improve influenza outcomes remains an important question for future studies.

Acknowledgements

We warmly acknowledge Steven A Kliewer (Department of Pharmacology, UT Southwestern Medical Center, Dallas, TX) and Laila Mselli Lakhal (Toxalim, Research Centre in Food Toxicology, UMR 1331, Inrae, Université de Toulouse, France) for the gift of *Nr1i2*$^{-/-}$ mice. We also thank Patrick Balaguer (Institut de Recherche en Cancérologie de Montpellier, Inserm U1194, Université Montpellier, France) for the discussion. We acknowledge the infrastructure ChemBioFrance (http://www.chembiofrance.org/) for providing compounds from the Chimiothèque Nationale. In particular, Kiet Tran (École Nationale Supérieure de Chimie de Montpellier) is warmly acknowledge for his assistance. These compounds (not described in the present study) were selected based on structural or functional similarities to IPA. Francisco Jimenez is acknowledged for the help on IHC staining. We thank members of the animal facility of the Institut Pasteur de Lille (PLETHA) for the technical assistance. The authors thank @BRIDGe platform (https://abridge.inrae.fr) for the PCR products sequencing and the ISC CRB-Anim (https://doi.org/10.15454/1.5613785622827378E12). We thank the ARIADNE-criblage platform for providing access to HCS equipements.

Funding

This work was supported in part by the Institut National de la Santé et de la Recherche Médicale (Inserm), Centre National de la Recherche Scientifique (CNRS), University of Lille, and Pasteur Institute of Lille. This work was supported by the Hauts-de-France Region through the action d'initiative régionale pour la recherche - volet Start-AIRR (IPA-VIR, DRESS-2024-011398), the banque public d'investissement bpifrance (contrat d'aide en subvention DOS0240769/00) and by the Université de Lille Excellence Initiative (V-startairr-24-006 and V-startairr-26-001, plan d'investissement France 2030). The IPA-VIR program also benefited from support provided by the European Union.

Author contribution

F.T. conceived and supervised the study. S.H. designed the figures and F.T. drafted the manuscript. S.H and F.T. designed the experiments, and S.H., C.B., C.V., L.D., P.B.R. performed the animal experiments. S.H. measured the pathological scores and viral loads and performed the RT-PCR. C.B, V.R. and J.M.C performed the 16S sequencing and made the bioinformatic analysis. F.G, P.M. and F.A. synthesized and analyzed the IPA analogues. S.H, A.T. and S.B. analyzed the potential antiviral effects of IPA and IPA analogues. B.H. analyzed the concentration of tryptophan derivatives in blood. I.W. provided critical comments. All authors discussed the results and revised the manuscript. F.T. obtained fundings.

Disclosure of potential conflict of interest

The authors declare that the research was conducted in the absence of any commercial or financial relationships that could be construed as a potential conflict of interest.

Data availability statement

The datasets generated and/or analyzed during this study are available from the corresponding author upon reasonable request. The sequence datasets (16S RNA sequencing) generated in this study are publicly available in the National Center for Biotechnology Information - Sequence Read Archive database under accession number: PRJNA1544808 (https://www.ncbi.nlm.nih.gov/bioproject/PRJNA1544808).

Legends for figures

Figure 1. Impact of *C. sporogenes* supplementation on IPA production and gut microbiota composition in IAV-infected mice. A, Schematic representation of the experimental procedure. Male C57BL/6 mice received DPBS-glycerol (Vh) or *C. sporogenes* (8 x10^7 CFU/mouse/day) in DPBS-glycerol, 7 days before IAV infection until the experimental endpoint. Mice were infected with IAV on day 0 and were sacrificed on 7 dpi. Non-infected vehicle-treated mice (Mock) served as controls. **B**, IPA was measured in blood samples using LC-MS /MS. (mean ± SD). Values for individual animal are presented (n = 6-9/group) (nM). One representative experiment out of four independent experiments is shown. Statistical significance was determined using a two-tailed Mann-Whitney U test. (** $p < 0.01$). **C**, Seven days after IAV infection, fecal contents were collected for 16S rRNA profiling (n = 9/group). Fecal samples from each mock-infected mouse were also collected (n = 6). Maslin2 analysis indicating the most discriminant bacterial genus associated with changes in *C. sporogenes*-treated mice. Only genera with a MaAsLin2 q-value < 0.25 are shown.

Figure 2. Effect of *C. sporogenes* administration prior to influenza infection on body weight loss, lung viral load and inflammation. **A**, Body weight loss during infection (expressed as percentage initial weight). The right panel shows area under the curve (AUC) at 7 dpi. **B**, Clinical scores were monitored over the 7-day infection period. The right panel shows AUC (cumulative welfare assessment score, CWAS). **C**, The number of infectious particles was quantified using a $TCID_{50}$ assay. Data are expressed as the mean ± SD of infectious virus particles per mL. **D**, Correlation between pulmonary viral load and IPA levels in blood was measured by Pearson's correlation analysis and linear regression in R. **E** and **G**, mRNA copy numbers were quantified by RT-PCR (7 dpi). Data are expressed as the mean fold change relative to average gene expression in mock-infected animals ± SD. **F**, Cytokine concentrations in blood as measured by ELISA. **A-G**, A single experiment out of three is shown (n = 9-10). Significant differences were determined using the two-tailed Mann Whitney *U* test (**A-C** and **E-F**). (* $p < 0.05$, ** $p < 0.01$, **** $p < 0.0001$).

Figure 3. Effect of IPA and its analogues on viral replication *in vitro*. **A** and **B**, Human A549 and mouse MLE12 lung epithelial cells were exposed to grading doses of IPA (1-1000 µM). **C**, Synthetic route to original carbazoles as IPA analogues. **D**, A549 cells were exposed with IPA analogues (75 µM). **A**, **B**, and **D**. One hour post-treatment, cells were infected with IAV (1 MOI). 24 h after infection, the percentage of IAV-positive cells as well as the number of living cells were quantified using an automated fluorescent confocal microscope. Amandatine (100 µM) was used as a positive control. Statistical significance was determined using a two-tailed Mann-Whitney *U* test. (* $p < 0.05$, *** $p < 0.001$, **** $p < 0.0001$).

Figure 4. Role of PXR signaling in the protective effects of *C. sporogenes* supplementation in IAV-infected mice. **A**, Representative micrographs showing PXR expression in the lungs by immunohistochemistry (x 20). **B**, mRNA copy n numbers were quantified by RT-PCR (whole lungs, mock and IAV-infected mice). Data are expressed as the mean fold change relative to average gene expression in mock-infected animals ± SD. One experiment out of at least four performed (n = 6-8). **C**, Wild type mice and *Nr1i2*$^{-/-}$ mice were infected with IAV. The body weight loss, clinical score, viral load and expression of genes in lungs are shown. **D**, Wild type mice and *Nr1i2*$^{-/-}$ mice were treated with *C. sporogenes* as described in **Figure. 1A** and then infected with IAV. **C** and **D**, One experiment out of two performed is shown (n = 7). Statistical significance was determined using a two-tailed Mann-Whitney *U* test. (*** $p < 0.001$, **** $p < 0.0001$).

Figure 5. Effect of pasteurized *C. sporogenes* administration on body weight loss, lung viral load and inflammation. **A** and **B**, Body weight loss and clinical scores were monitored over the 7-day period. Data are expressed as AUC. **C**, The number of infectious particles was quantified using a $TCID_{50}$ assay. Data are expressed as the mean ± SD of infectious virus particles per mL. **D**,

Concentration of IPA in blood and correlation with viral load in lungs. **E** and **G**, mRNA copy numbers were quantified by RT-PCR (7 dpi). The data are expressed as the mean fold change relative to average gene expression in mock-infected animals ± SD. **F**, Concentration of cytokines in blood. **A-G**, one experiment shown out of three performed (n = 8-9). Significant differences were determined using the two-tailed Mann Whitney U test (* $P \leq 0.05$, ** $P < 0.01$, *** $P \leq 0.001$). **H**, Seven days after IAV infection, fecal contents were collected for 16S rRNA profiling (n = 8/group). Fecal samples from each mock-infected mouse were also collected (n = 6). MaAsLin2 analysis showing bacterial genera differentially associated with pasteurized *C. sporogenes* treatment compared with vehicle at 7 dpi. Only genera with a MaAsLin2 q-value < 0.25 are shown.

Supplementary Figure 1. A, Body schematic showing the conversion pathway of tryptophan into different bioactive indole metabolites including those that require the gut microbiota for conversion. **B**, ILA and IAA were measured in blood samples using targeted quantitative metabolomics (mean ± SD). Values for each individual animal are presented (n = 9) (nM).**C**, Fecal contents were collected the day of infection and at 7 dpi for 16S rRNA profiling. Maslin2 analysis indicating the most discriminant bacterial genus associated with changes in IAV-infected mice (Vh *versus C. sporogenes*-treated mice). Only genera with a MaAsLin2 q-value < 0.25 are shown.

Supplementary Figure 2. **Effect of *C. sporogenes* supplementation on systemic kynurenin-to-tryptophan ratio and gene expression in colon**. **A**, Correlation between body weight loss and clinical scores was measured by Pearson's correlation analysis and linear regression in R. **B**, Systemic kynurenin/tryptophan ratio in vehicle and *C. sporogenes*-treated mice at 7 dpi. **C**, Colons were collected at 7 dpi. mRNA copy numbers were quantified by RT-PCR. Data are expressed as the mean fold change relative to average gene expression in mock-infected animals ± SD. A single experiment out of three was performed (n = 9-10). Significant differences were determined using the two-tailed Mann Whitney U test (* $p < 0.05$).

Supplementary Figure 3. Effect of pasteurized *C. sporogenes* administration prior to influenza infection on body weight loss, lung viral load and inflammation. **A**, Correlation between body weight loss and clinical scores was measured by Pearson's correlation analysis and linear regression in R. **B**, ILA and IAA were measured in blood samples using targeted quantitative metabolomics (mean ± SD). Values for individual animal are presented (nM). **C**, Systemic kynurenin/tryptophan ratio in vehicle and *C. sporogenes*-treated mice at 7 dpi. **D**, mRNA copy numbers were quantified by RT-PCR (7 dpi). Data are expressed as the mean fold change relative to average gene expression in mock-infected animals ± SD. One experiment shown out of three performed (n = 8-9). Significant differences were determined using the two-tailed Mann Whitney U test (* $p < 0.05$, ** $p < 0.01$, *** $p < 0.001$).

Supplementary Figure 4. Structure of intermediate **26** identified by J. Bergman and A.-L. Johnson, **7**, and its 4-oxo isomer **7'**.

References

1. Peteranderl, C., Herold, S. & Schmoldt, C. Human Influenza Virus Infections. *Semin. Respir. Crit. Care Med.* **37**, 487–500 (2016).

2. Xie, Y., Choi, T. & Al-Aly, Z. Long-term outcomes following hospital admission for COVID-19 versus seasonal influenza: a cohort study. *Lancet Infect. Dis.* **24**, 239–255 (2024).

3. Taubenberger, J. K. & Morens, D. M. 1918 Influenza: the mother of all pandemics. *Emerg. Infect. Dis.* **12**, 15–22 (2006).

4. Ichinohe, T. *et al.* Microbiota regulates immune defense against respiratory tract influenza A virus infection. *Proc. Natl. Acad. Sci. U. S. A.* **108**, 5354–5359 (2011).

5. Samuelson, D. R., Welsh, D. A. & Shellito, J. E. Regulation of lung immunity and host defense by the intestinal microbiota. *Front. Microbiol.* **6**, 1085 (2015).

6. Dang, A. T. & Marsland, B. J. Microbes, metabolites, and the gut-lung axis. *Mucosal Immunol.* **12**, 843–850 (2019).

7. Sencio, V., Machado, M. G. & Trottein, F. The lung–gut axis during viral respiratory infections: the impact of gut dysbiosis on secondary disease outcomes. *Mucosal Immunol.* **14**, 296–304 (2021).

8. Abt, M. C. *et al.* Commensal bacteria calibrate the activation threshold of innate antiviral immunity. *Immunity* **37**, 158–170 (2012).

9. Steed, A. L. *et al.* The microbial metabolite desaminotyrosine protects from influenza through type I interferon. *Science* **357**, 498–502 (2017).

10. Bradley, K. C. *et al.* Microbiota-Driven Tonic Interferon Signals in Lung Stromal Cells Protect from Influenza Virus Infection. *Cell Rep.* **28**, 245-256.e4 (2019).

11. Stefan, K. L., Kim, M. V., Iwasaki, A. & Kasper, D. L. Commensal Microbiota Modulation of Natural Resistance to Virus Infection. *Cell* **183**, 1312-1324.e10 (2020).

12. Deriu, E. *et al.* Influenza Virus Affects Intestinal Microbiota and Secondary Salmonella Infection in the Gut through Type I Interferons. *PLoS Pathog.* **12**, e1005572 (2016).

13. Yildiz, S., Mazel-Sanchez, B., Kandasamy, M., Manicassamy, B. & Schmolke, M. Influenza A virus infection impacts systemic microbiota dynamics and causes quantitative enteric dysbiosis. *Microbiome* **6**, 9 (2018).

14. Sencio, V. *et al.* Gut Dysbiosis during Influenza Contributes to Pulmonary Pneumococcal Superinfection through Altered Short-Chain Fatty Acid Production. *Cell Rep.* **30**, 2934-2947.e6 (2020).

15. Sencio, V. *et al.* Influenza Virus Infection Impairs the Gut's Barrier Properties and Favors Secondary Enteric Bacterial Infection through Reduced Production of Short-Chain Fatty Acids. *Infect. Immun.* **89**, e0073420 (2021).

16. Heumel, S. *et al.* Shotgun metagenomics and systemic targeted metabolomics highlight indole-3-propionic acid as a protective gut microbial metabolite against influenza infection. *Gut Microbes* **16**, 2325067 (2024).

17. Qin, N. *et al.* Influence of H7N9 virus infection and associated treatment on human gut microbiota. *Sci. Rep.* **5**, 14771 (2015).

18. Gu, S. *et al.* Alterations of the Gut Microbiota in Patients With Coronavirus Disease 2019 or H1N1 Influenza. *Clin. Infect. Dis. Off. Publ. Infect. Dis. Soc. Am.* **71**, 2669–2678 (2020).

19. Fuentes, S. *et al.* Associations of faecal microbiota with influenza-like illness in participants aged 60 years or older: an observational study. *Lancet Healthy Longev.* **2**, e13–e23 (2021).

20. Dodd, D. *et al.* A gut bacterial pathway metabolizes aromatic amino acids into nine circulating metabolites. *Nature* **551**, 648–652 (2017).

21. Krause, F. F. *et al.* Clostridium sporogenes-derived metabolites protect mice against colonic inflammation. *Gut Microbes* **16**, 2412669 (2024).

22. Du, L., Qi, R., Wang, J., Liu, Z. & Wu, Z. Indole-3-Propionic Acid, a Functional Metabolite of Clostridium sporogenes, Promotes Muscle Tissue Development and Reduces Muscle Cell Inflammation. *Int. J. Mol. Sci.* **22**, 12435 (2021).

23. Wang, Z. *et al.* The gut microbiota-derived metabolite indole-3-propionic acid enhances leptin sensitivity by targeting STAT3 against diet-induced obesity. *Clin. Transl. Med.* **14**, e70053 (2024).

24. Li, Q. *et al.* Microbial metabolite indole-3-propionic acid drives mitochondrial respiration in CD4+ T cells to confer protection against intestinal inflammation. *Nat. Metab.* **7**, 2510–2530 (2025).

25. Serger, E. *et al.* The gut metabolite indole-3 propionate promotes nerve regeneration and repair. *Nature* **607**, 585–592 (2022).

26. Li, L. *et al.* Synbiotic therapy with Clostridium sporogenes and xylan promotes gut-derived indole-3-propionic acid and improves cognitive impairments in an Alzheimer's disease mouse model. *Food Funct.* **15**, 7865–7882 (2024).

27. Xiao, H.-W. *et al.* Gut microbiota-derived indole 3-propionic acid protects against radiation toxicity via retaining acyl-CoA-binding protein. *Microbiome* **8**, 69 (2020).

28. Qi, Z. *et al.* Intermittent fasting inhibits platelet activation and thrombosis through the intestinal metabolite indole-3-propionate. *Life Metab.* **4**, loaf002 (2025).

29. Wang, S. *et al.* Indole-3-propionic acid alleviates sepsis-associated acute liver injury by activating pregnane X receptor. *Mol. Med.* **29**, 65 (2023).

30. Staudinger, J. L. *et al.* The nuclear receptor PXR is a lithocholic acid sensor that protects against liver toxicity. *Proc. Natl. Acad. Sci. U. S. A.* **98**, 3369–3374 (2001).

31. NOLAND, W. E. & HAMMER, C. F. A Novel Rearrangement Involving Indole Dimers1. *J. Org. Chem.* **25**, 1536–1542 (1960).

32. Mallick, H. *et al.* Multivariable association discovery in population-scale meta-omics studies. *PLoS Comput. Biol.* **17**, e1009442 (2021).

33. Pett, S. L. *et al.* Increased Indoleamine-2,3-Dioxygenase Activity Is Associated With Poor Clinical Outcome in Adults Hospitalized With Influenza in the INSIGHT FLU003Plus Study. *Open Forum Infect. Dis.* **5**, ofx228 (2018).

34. Pizzini, A. *et al.* Assessment of neopterin and indoleamine 2,3-dioxygenase activity in patients with seasonal influenza: A pilot study. *Influenza Other Respir. Viruses* **13**, 603–609 (2019).

35. Short, K. R. *et al.* Influenza virus damages the alveolar barrier by disrupting epithelial cell tight junctions. *Eur. Respir. J.* **47**, 954–966 (2016).

36. Gao, H. *et al.* Microbiota-derived IPA alleviates intestinal mucosal inflammation through upregulating Th1/Th17 cell apoptosis in inflammatory bowel disease. *Gut Microbes* **17**, 2467235 (2025).

37. Zhao, X. *et al.* 3-Indoleacetonitrile Is Highly Effective in Treating Influenza A Virus Infection In Vitro and In Vivo. *Viruses* **13**, 1433 (2021).

38. Brancato, V. *et al.* Design of inhibitors of influenza virus membrane fusion: synthesis, structure-activity relationship and in vitro antiviral activity of a novel indole series. *Antiviral Res.* **99**, 125–135 (2013).

39. Hattori, S.-I. *et al.* GRL-0920, an Indole Chloropyridinyl Ester, Completely Blocks SARS-CoV-2 Infection. *mBio* **11**, e01833-20 (2020).

40. Piscotta, F. J. *et al.* Metabolites with SARS-CoV-2 Inhibitory Activity Identified from Human Microbiome Commensals. *mSphere* **6**, e0071121 (2021).

41. Chauhan, J. *et al.* Development of indolealkylamine derivatives as potential multi-target agents for COVID-19 treatment. *Eur. J. Med. Chem.* **249**, 115152 (2023).

42. Schütz, B. *et al.* Modulation of Host Immunity by Microbiome-Derived Indole-3-Propionic Acid and Other Bacterial Metabolites. *Eur. J. Immunol.* **55**, e202451594 (2025).

43. Bergman, J. & Johnson, A.-L. A Short Synthesis of the Carbazole Alkaloid Clausine E. *Org. Prep. Proced. Int.* **38**, 593–599 (2006).

44. Pulakazhi Venu, V. K. *et al.* The pregnane X receptor and its microbiota-derived ligand indole 3-propionic acid regulate endothelium-dependent vasodilation. *Am. J. Physiol. Endocrinol. Metab.* **317**, E350–E361 (2019).

45. Peng, R. *et al.* Gut Clostridium sporogenes-derived indole propionic acid suppresses osteoclast formation by activating pregnane X receptor. *Pharmacol. Res.* **202**, 107121 (2024).

46. Chollet, L. *et al.* Faecalibacterium duncaniae as a novel next generation probiotic against influenza. *Front. Immunol.* **15**, 1347676 (2024).

47. Antunes Fernandes, K. *et al.* Maternal helminths rewire the microbiota to promote offspring antiviral immunity. *Cell Host Microbe* **34**, 1050-1066.e9 (2026).

48. Chen, Y. *et al.* Six-month follow-up of gut microbiota richness in patients with COVID-19. *Gut* **71**, 222–225 (2022).

49. Yao, L. *et al.* Dysrupted microbial tryptophan metabolism associates with SARS-CoV-2 acute inflammatory responses and long COVID. *Gut Microbes* **16**, 2429754 (2024).

50. Kullberg, R. F. J. *et al.* Effect of the gut microbiota-derived tryptophan metabolite indole-3-acetic acid in pneumonia. *Nat. Commun.* **16**, 8565 (2025).

51. Mahooti, M. *et al.* Immunomodulatory and prophylactic effects of Bifidobacterium bifidum probiotic strain on influenza infection in mice. *World J. Microbiol. Biotechnol.* **35**, 91 (2019).

52. Lu, W. *et al.* The Potential Role of Probiotics in Protection against Influenza a Virus Infection in Mice. *Foods* **10**, 902 (2021).

53. Han, M. *et al.* Oral co-administration of Lactiplantibacillus plantarum 16 and Lacticaseibacillus rhamnosus P118 improves host defense against influenza A virus infection. *J. Virol.* **98**, e0095024 (2024).

54. Niu, J. *et al.* Microbiota-derived acetate enhances host antiviral response via NLRP3. *Nat. Commun.* **14**, 642 (2023).

55. Zünd, J. N. *et al.* Novel cross-feeding human gut microbes metabolizing tryptophan to indole-3-propionate. *Gut Microbes* **17**, 2501195 (2025).

56. Jia, D. *et al.* Microbial metabolite enhances immunotherapy efficacy by modulating T cell stemness in pan-cancer. *Cell* **187**, 1651-1665.e21 (2024).

57. Fan, W. *et al.* Indole-acetaldehyde from Rothia mucilaginosa activates the PXR/NRF2 axis to enhance alveolar macrophage phagocytosis and protect against ARDS. *Respir. Res.* **27**, 112 (2026).

58. Negatu, D. A. *et al.* Whole-Cell Screen of Fragment Library Identifies Gut Microbiota Metabolite Indole Propionic Acid as Antitubercular. *Antimicrob. Agents Chemother.* **62**, e01571-17 (2018).

59. Pan, Y. *et al.* Hepcidin sustains Kupffer cell immune defense against bloodstream bacterial infection via gut-derived metabolites in mice. *J. Clin. Invest.* **135**, e189607 (2025).

60. Robinson, D. P., Lorenzo, M. E., Jian, W. & Klein, S. L. Elevated 17β-estradiol protects females from influenza A virus pathogenesis by suppressing inflammatory responses. *PLoS Pathog.* **7**, e1002149 (2011).

Figures

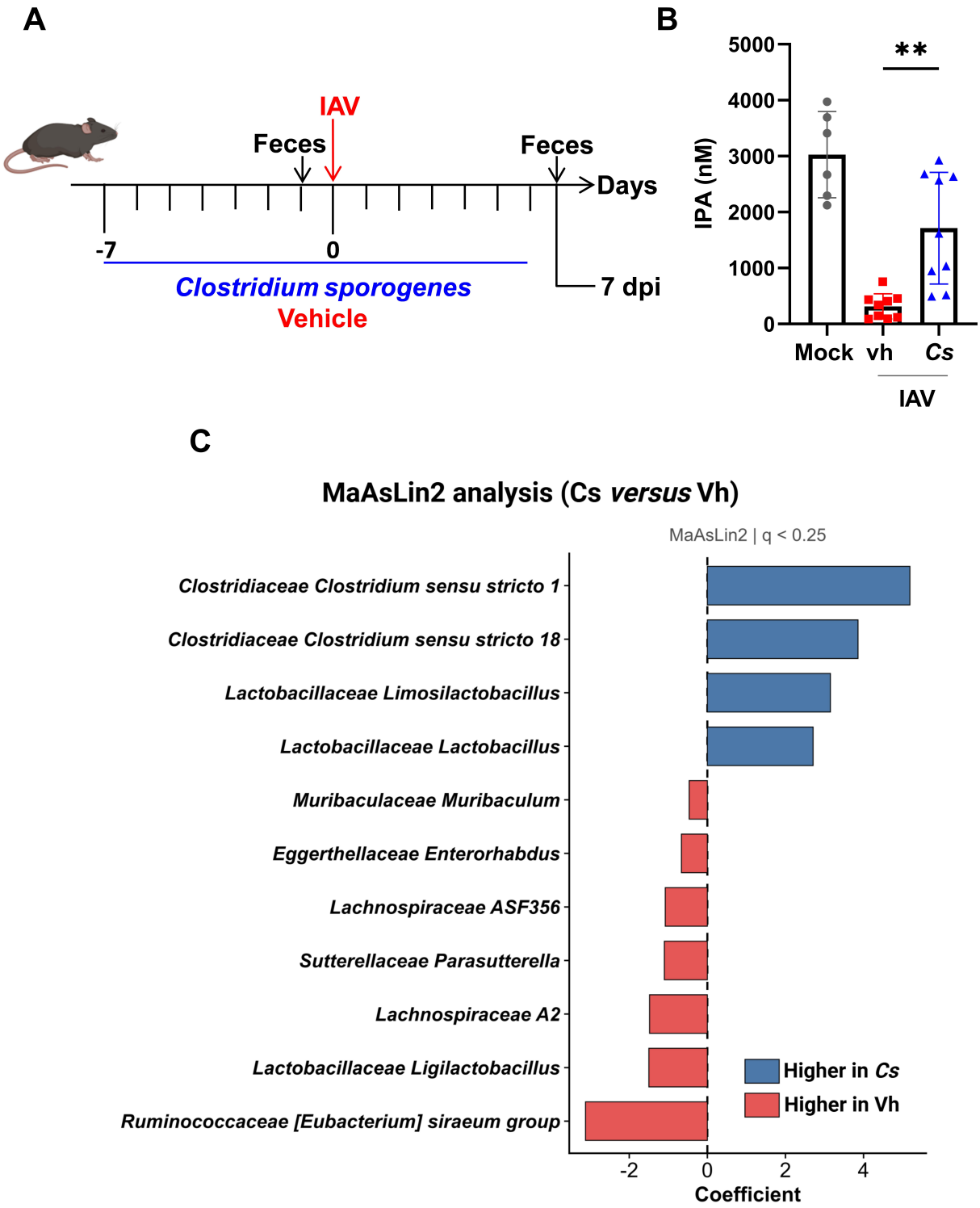


Figure 1

Impact of *C. sporogenes* supplementation on IPA production and gut microbiota composition in IAV-infected mice. A, Schematic representation of the experimental procedure. Male C57BL/6 mice received DPBS-glycerol (Vh) or *C. sporogenes* (8 x10^7 CFU/mouse/day) in DPBS-glycerol, 7 days before IAV

infection until the experimental endpoint. Mice were infected with IAV on day 0 and were sacrificed on 7 dpi. Non-infected vehicle-treated mice (Mock) served as controls. **B**, IPA was measured in blood samples using LC-MS /MS. (mean ± SD). Values for individual animal are presented (*n* = 6-9/group) (nM). One representative experiment out of four independent experiments is shown. Statistical significance was determined using a two-tailed Mann-Whitney *U* test. (** $p < 0.01$). **C**, Seven days after IAV infection, fecal contents were collected for 16S rRNA profiling (*n* = 9/group). Fecal samples from each mock-infected mouse were also collected (*n* = 6). Maslin2 analysis indicating the most discriminant bacterial genus associated with changes in *C. sporogenes*-treated mice. Only genera with a MaAsLin2 q-value < 0.25 are shown.

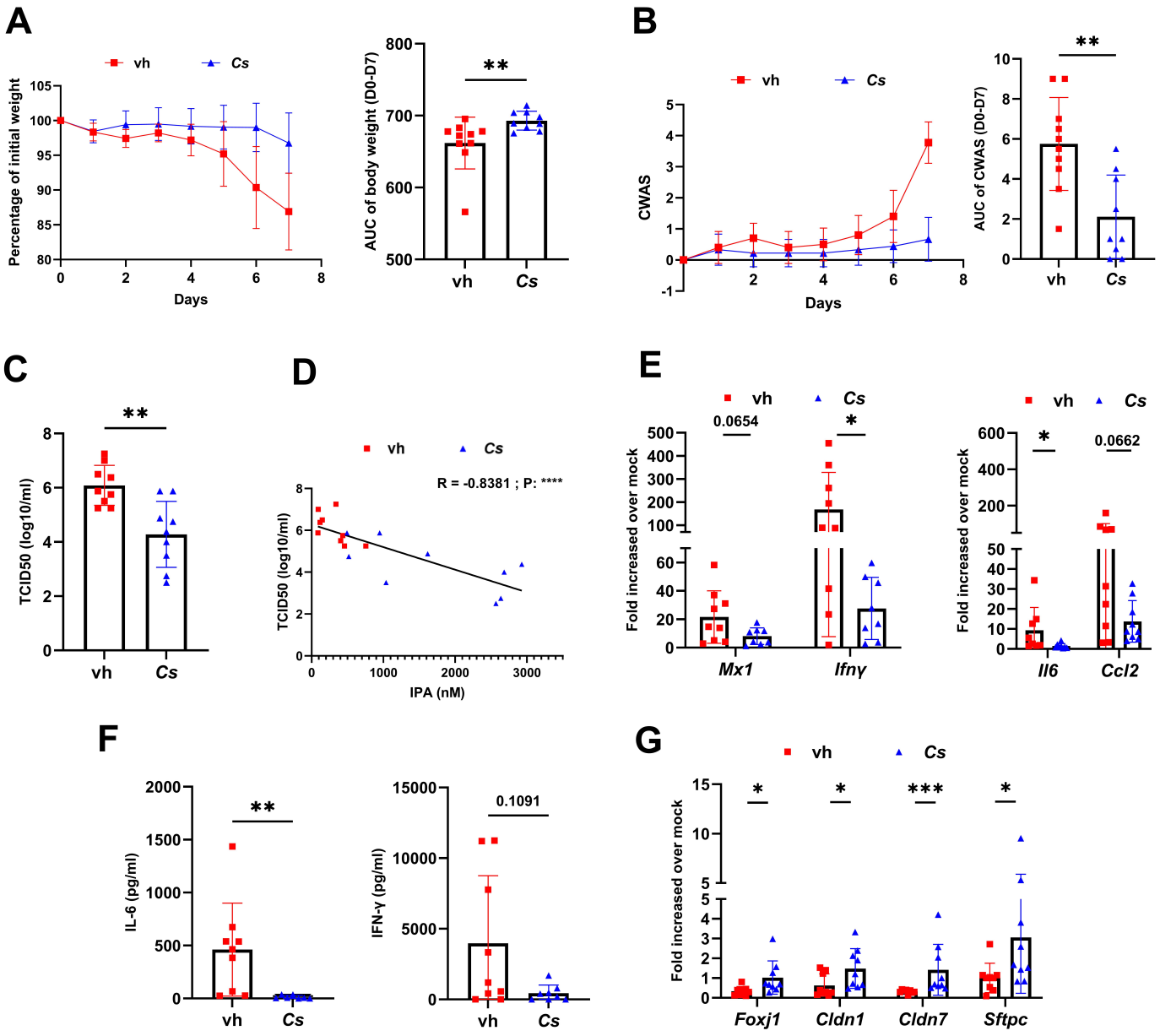


Figure 2

Effect of *C. sporogenes* administration prior to influenza infection on body weight loss, lung viral load and inflammation. A, Body weight loss during infection (expressed as percentage initial weight). The right panel shows area under the curve (AUC) at 7 dpi. **B**, Clinical scores were monitored over the 7-day infection period. The right panel shows AUC (cumulative welfare assessment score, CWAS). **C**, The number of infectious particles was quantified using a $TCID_{50}$ assay. Data are expressed as the mean ± SD of infectious virus particles per mL. **D**, Correlation between pulmonary viral load and IPA levels in blood was measured by Pearson's correlation analysis and linear regression in R. **E** and **G**, mRNA copy numbers were quantified by RT-PCR (7 dpi). Data are expressed as the mean fold change relative to average gene expression in mock-infected animals ± SD. **F**, Cytokine concentrations in blood as measured by ELISA. **A-G**, A single experiment out of three is shown (n = 9-10). Significant differences were determined using the two-tailed Mann Whitney *U* test (**A**-**C** and **E-F**). (* $p < 0.05$, ** $p < 0.01$, **** $p < 0.0001$).

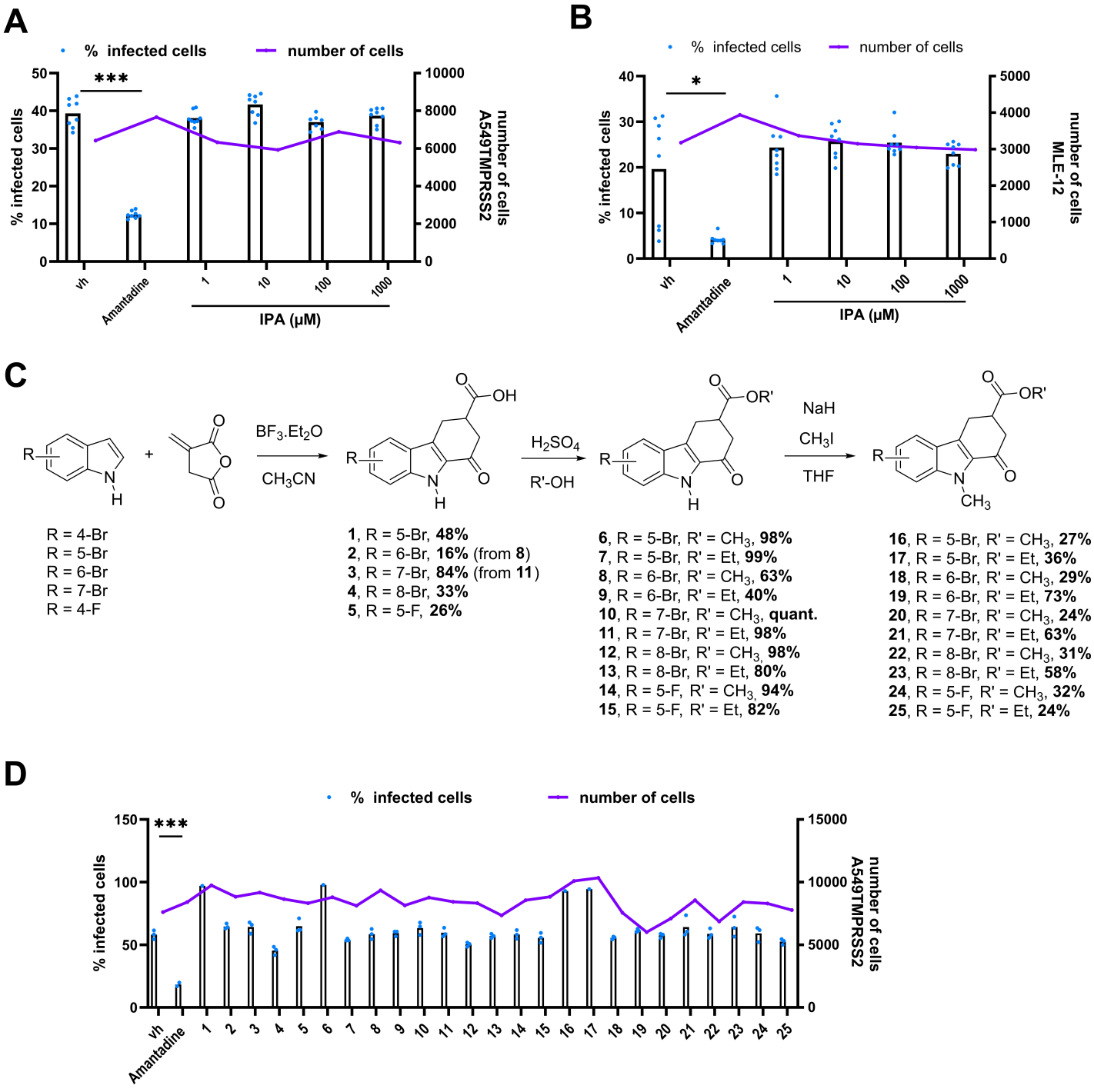


Figure 3

Effect of IPA and its analogues on viral replication *in vitro*. **A** and **B**, Human A549 and mouse MLE12 lung epithelial cells were exposed to grading doses of IPA (1-1000 mM). **C**, Synthetic route to original carbazoles as IPA analogues. **D**, A549 cells were exposed with IPA analogues (75 mM). **A**, **B**, and **D**. One hour post-treatment, cells were infected with IAV (1 MOI). 24 h after infection, the percentage of IAV-positive cells as well as the number of living cells were quantified using an automated fluorescent

confocal microscope. Amandatine (100 µM) was used as a positive control. Statistical significance was determined using a two-tailed Mann-Whitney *U* test. (* $p < 0.05$, *** $p < 0.001$, **** $p < 0.0001$).

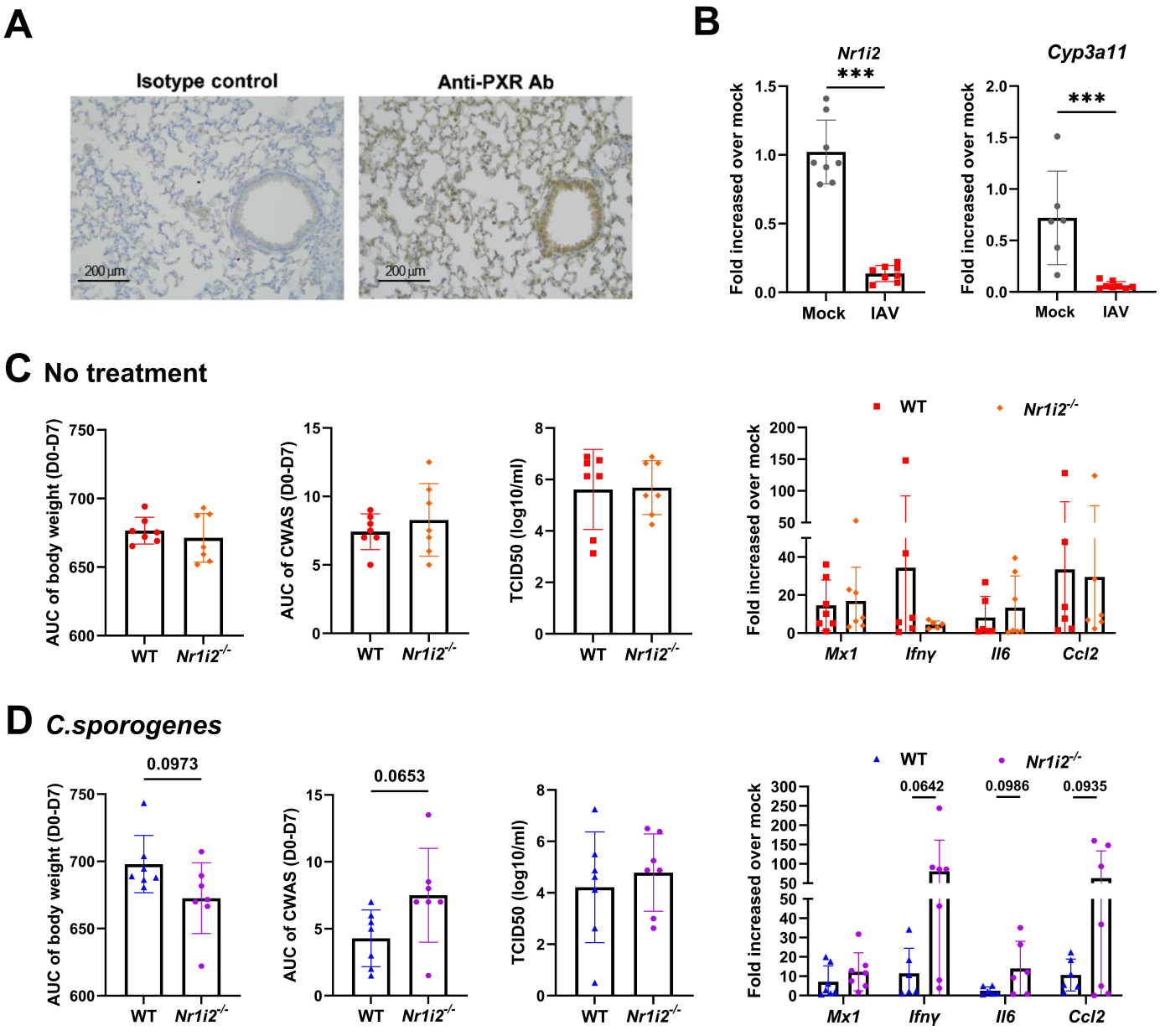


Figure 4

Role of PXR signaling in the protective effects of *C. sporogenes* supplementation in IAV-infected mice. **A**, Representative micrographs showing PXR expression in the lungs by immunohistochemistry (x 20). **B**, mRNA copy n numbers were quantified by RT-PCR (whole lungs, mock and IAV-infected mice). Data are expressed as the mean fold change relative to average gene expression in mock-infected animals ± SD. One experiment out of at least four performed (n = 6-8). **C**, Wild type mice and *Nr1i2*$^{-/-}$ mice were infected with IAV. The body weight loss, clinical score, viral load and expression of genes in lungs are shown. **D**, Wild type mice and *Nr1i2*$^{-/-}$ mice were treated with *C. sporogenes* as described in **Figure. 1A** and then

infected with IAV. **C** and **D**, One experiment out of two performed is shown (n = 7). Statistical significance was determined using a two-tailed Mann-Whitney U test. (*** $p < 0.001$, **** $p < 0.0001$).

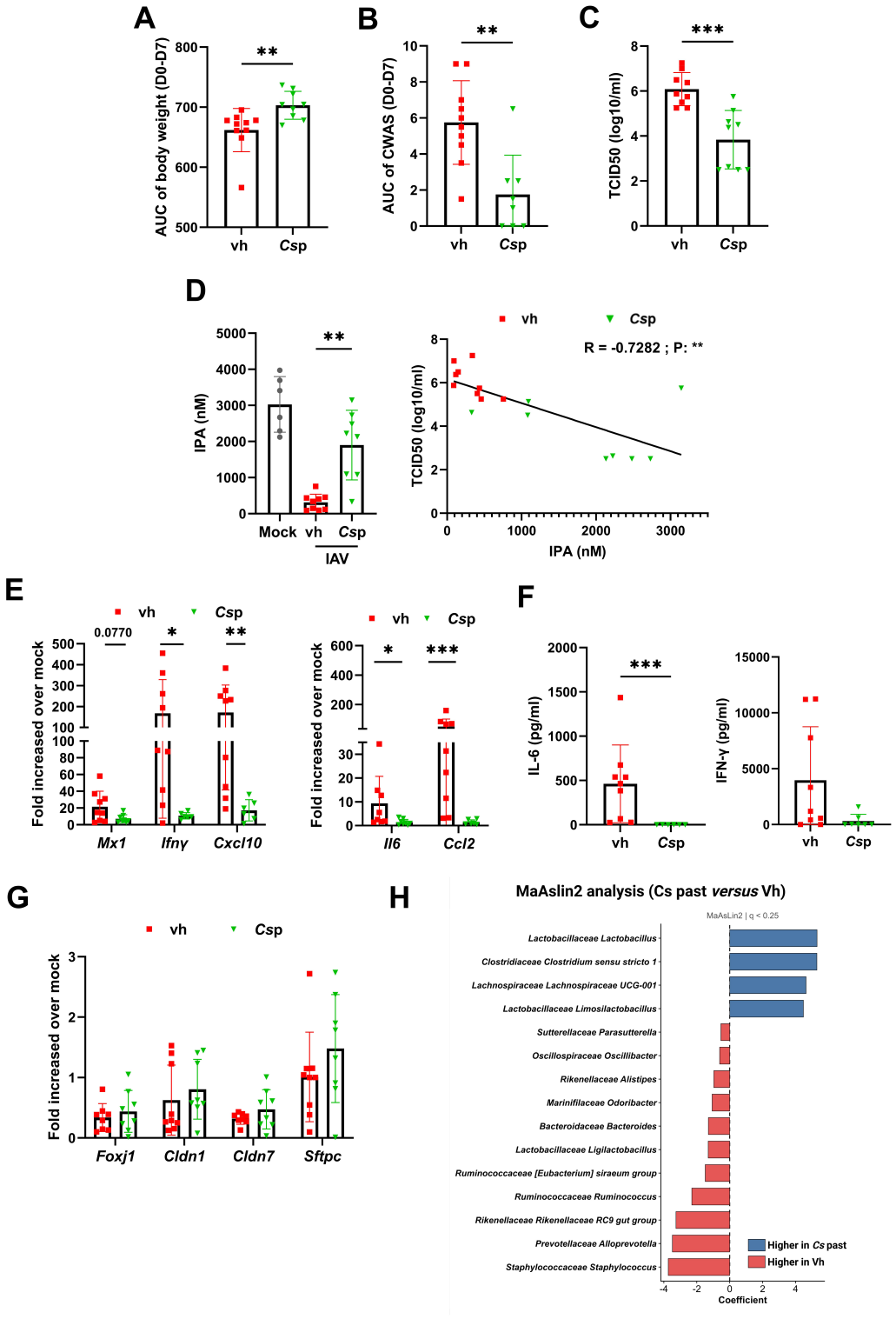


Figure 5

Effect of pasteurized *C. sporogenes* administration on body weight loss, lung viral load and inflammation. A and **B**, Body weight loss and clinical scores were monitored over the 7-day period. Data

are expressed as AUC. **C**, The number of infectious particles was quantified using a $TCID_{50}$ assay. Data are expressed as the mean ± SD of infectious virus particles per mL. **D**, Concentration of IPA in blood and correlation with viral load in lungs. **E** and **G**, mRNA copy numbers were quantified by RT-PCR (7 dpi). The data are expressed as the mean fold change relative to average gene expression in mock-infected animals ± SD. **F**, Concentration of cytokines in blood. **A**-**G**, one experiment shown out of three performed (n = 8-9). Significant differences were determined using the two-tailed Mann Whitney U test (* $P \leq 0.05$, ** $P < 0.01$, *** $P \leq 0.001$). **H**, Seven days after IAV infection, fecal contents were collected for 16S rRNA profiling (n = 8/group). Fecal samples from each mock-infected mouse were also collected (n = 6). MaAsLin2 analysis showing bacterial genera differentially associated with pasteurized *C. sporogenes* treatment compared with vehicle at 7 dpi. Only genera with a MaAsLin2 q-value < 0.25 are shown.

Supplementary Files

This is a list of supplementary files associated with this preprint. Click to download.

- Table1.docx
- Table2.docx
- Table3.docx
- Figure1sup.jpg
- Figure2sup.jpg
- Figure3sup.jpg
- supplementarymaterialsandmethods.docx